

Modeling of perforated plates and screens using rigid frame porous models

Noureddine Atalla^a, Franck Sgard^{b,*}

^aGAUS, Department of Mechanical Engineering, Univ. de Sherbrooke, Sherbrooke, Que., Canada J1K 2R1

^bLaboratoire des Sciences de l'Habitat, DGCB URA CNRS 1652, Ecole Nationale des Travaux Publics de l'Etat, 69518 Vaulx-en-Velin Cedex, France

Received 5 September 2006; received in revised form 8 January 2007; accepted 10 January 2007

Available online 7 March 2007

Abstract

There are several models and approaches for predicting the acoustic response of perforated plates and screens. Classical models are devoted to specific configurations: particular geometrical parameters including the size and shape of the perforations, excitations type, mounting of the screen (bonded vs. free), and interfacing media involved in multilayers sound packages. This paper reviews these models and presents a simple and general model that can handle easily and automatically the miscellaneous configurations in the context of the transfer matrix method. In particular, it is shown that a perforated plate or screen can be modeled as an equivalent fluid following the Johnson–Allard approach with an equivalent tortuosity. This equivalent tortuosity is shown to depend on the media interfacing with the perforated system. Experimental results depicting various practical configurations are shown to corroborate the validity of the proposed model and to evaluate its performance compared to classical ones.

© 2007 Elsevier Ltd. All rights reserved.

1. Introduction

Perforated plates and screens are widely used in various noise control applications. They are mainly used as protective layers of porous materials. When the radius of the perforations ranges between 1 mm and 1 cm, one generally speaks of *macro-perforated* systems. For submillimetric radius, the term *micro-perforated* panel is rather used. Screens are characterized by their porosity and flow resistivity, which are, of course related, to the size of the perforation and the perforation rate. Typical screen resistivities and porosities are between 10^3 and 10^6 N s m^{-4} and 1% and 80%, respectively.

The acoustic effect of perforated panels and screens is mainly dependent on their perforation rate or porosity, their perforation size or flow resistivity, their perforation thickness and their mounting conditions. The perforated plate motion can also play a role. This is; however, dependent on the thickness and mounting conditions; usually stiffness is neglected and only inertia is accounted for. Depending on their design, screens and perforated plates can affect the acoustic behavior of the material, which they are coupled to. For example,

*Corresponding author. Tel.: +1 514 288 1551; fax: +1 514 2889 399.

E-mail address: frasga@irsst.qc.ca (F. Sgard).

resistive screens can enhance the low-frequency sound absorption performance of low-flow resistivity materials if not completely bonded. At high frequencies; however, they may decrease the sound absorption coefficient of the protected material depending on the mounting conditions [1]. Perforated panels combined with air gaps or porous materials can also be used as efficient sound absorbers or sound attenuators in given frequency bands if appropriately designed [1–4].

Numerous works have been devoted to the modeling of the acoustic impedance of such systems. A typically studied configuration consists of a flat rigid surface with periodically arranged holes. The associated classical modeling approach concentrates on the calculation of the acoustic impedance of one hole and its averaging using the fraction of perforated open area [2]. Several variants consider the interaction of a perforated system with a backing cavity filled or not with a porous material [1,3–9]. Recent generalizations consider the interaction of perforated systems with stratified porous media under normal and random incidence conditions [1,3–6,8], the effects of the diffraction phenomenon caused by impedance discontinuities of the boundary surface [7], the effect of interaction between perforations [9]. These various models are devoted to specific configurations: particular geometrical parameters including the size and shape of the perforations, excitations type, mounting of the screen (bonded vs. free), and interfacing media involved in multilayers sound packages.

This paper is an extended version of a talk presented at the 12th ICSV Meeting in Lisbon 2005 [10]. It presents a simple and general methodology that can handle easily and automatically these miscellaneous configurations in the context of the transfer matrix method. In particular, it is shown that a perforated plate or screen can be modeled as an equivalent fluid following the Johnson–Allard approach with an equivalent tortuosity. This effective tortuosity is shown to be a function of the correction length induced by the radiation of the perforated panel in free air and of the dynamic tortuosity of the media interfacing with it. Classical models for both perforated plates and screens including sub-millimeter perforations configurations can be reobtained using this simple approach. Comparisons between the present approach, classical models and experimental results carried out for normal incidence absorption coefficient corroborate its validity and versatility.

The paper is organized as follows. Firstly, an equivalent fluid model of the perforated panel based on Allard Johnson’s theory of porous media is presented. The model parameters are obtained in the typical cases where the perforated panel is coupled to free air, air gap or porous layers. Then, the validity of the approach is discussed by comparing prediction results obtained for normal incidence sound absorption coefficients with other existing models and measurements in various configurations. Finally, the conclusion summarizes the main results of this paper.

2. Normal surface impedance of a perforated panel

This section shows how some classical existing models for perforated panels can be recovered from an equivalent fluid model. Since it is shown that the coupling of the perforated panel with its surroundings amounts to a modification of its tortuosity depending on the medium in which it radiates, the correction term is presented in different configurations. It starts from the expression of the surface impedance of a plate made up of cylinders radiating into 2 semi-infinite media expressed in terms of Johnson–Allard’s acoustic parameters. The perforated plate is then coupled to other media such as a backing cavity filled or not with a porous layer. The case of a resistive perforated screen is finally tackled to show that the classical model (i.e. simple addition of the resistance of the screen) may be not sufficient if the perforated screen is coupled to an absorbing layer.

2.1. Case of a perforated panel coupled to semi-infinite fluid media

The perforated plate is assumed to be of infinite lateral extent and coupled on both sides to semi-infinite fluid media (see Fig. 1).

The physical phenomena involved in a perforated panel are well known and recalled in Fig. 2. The classical approaches consist in evaluating the normal surface impedance of the perforated plate backed by a semi-infinite fluid or a cavity starting from the surface impedance of a single perforation. The resistive part is

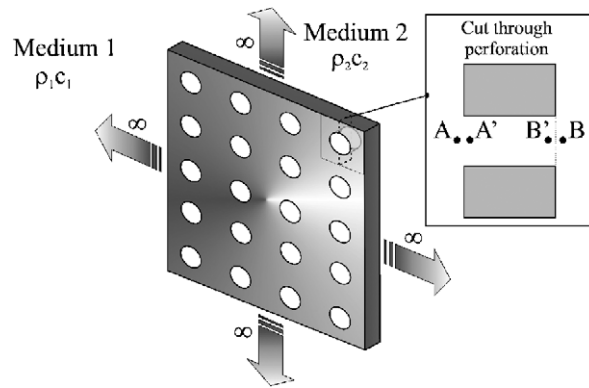


Fig. 1. Configuration of interest: perforated plate excited by a plane wave and backed by an infinite fluid medium.

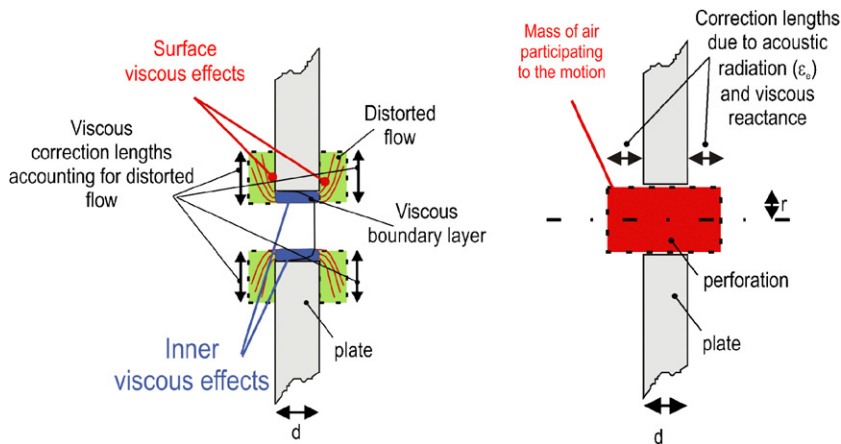


Fig. 2. Physical phenomena involved in a perforated plate.

induced by the viscous effects occurring within the perforation due to the viscous boundary layer and around its edges at the panel surface due to the distortion of the acoustic flow. The reactive part accounts for the motion of an air cylinder, which is thicker than the perforation depth. This is because of the mass loading associated to the sound radiation of the perforation and to the distortion of the acoustic flow at the panel surface, which contribute to make the air in the neck *heavier* and more difficult to move. This inertial effect amounts to increasing the mass of the vibrating air and is accounted for using correction lengths, which need to be added to the neck depth. The differences between the existing models reside both in the expressions of the viscous dissipation part (resistance) and the inertial part (reactance) according to the ratio of the perforation size and the acoustic wavelength.

To simplify the derivation, the perforation of the plate is assumed of cylindrical shape (thickness: d ; radius: r) and impinged by a normal incidence plane wave. Thus, the Biot's parameters for cylindrical pores parallel to the wave direction of propagation can be utilized. For straight cylindrical pores it has been shown [5] that the viscous and the thermal characteristics lengths, A and A' , respectively, are equal to the hydraulic radius of the pores, that is $A = A' = r$. The flow resistivity σ is related to the perforation radius r and to the perforation rate ϕ by $\sigma = 8\eta/\phi r^2$, where η is the dynamic viscosity of air. Due to the small thickness and shape of the pores, thermal effects are negligible. The impedance $Z_{A'}$, at the front face, inside a perforation at point A' (see Fig. 1), is mainly governed by the viscous and inertial effects. Both effects are accounted for in the expression of the effective density $\tilde{\rho}_e$. For acoustic wavelengths much larger than the plate thickness, the normal surface

impedance $Z_{A'}$ at circular frequency ω writes

$$Z_{A'} = j\omega\tilde{\rho}_e d + \phi Z_B, \quad (1)$$

where Z_B is the free air acoustic impedance of the backing medium. The effective density $\tilde{\rho}_e$ is linked to the air density ρ_0 by the dynamic tortuosity $\tilde{\alpha}$ ($\tilde{\rho}_e = \rho_0\tilde{\alpha}$) and reads [5]

$$\tilde{\rho}_e = \rho_0\alpha_\infty \left(1 + \frac{\sigma\phi}{j\omega\rho_0\alpha_\infty} G_J(\omega) \right) \quad (2)$$

with

$$G_J(\omega) = \left(1 + j \frac{4\omega\rho_0\alpha_\infty^2\eta}{\sigma^2\phi^2 A^2} \right)^{1/2}. \quad (3)$$

and α_∞ denotes the geometrical tortuosity. Consider now both the low- and high-frequency limits of $\tilde{\rho}_e$. These asymptotic behaviors correspond to millimetric and sub-millimetric perforation radii, respectively.

The high-frequency expression of $\tilde{\rho}_e$ is given by [5]

$$\tilde{\rho}_e = \rho_0\tilde{\alpha} = \alpha_\infty\rho_0 \left(1 + \frac{\delta}{A} \right) - j\alpha_\infty\rho_0 \frac{\delta}{A}. \quad (4)$$

Here

$$\delta = \sqrt{\frac{2\eta}{\rho_0\omega}},$$

represents the viscous boundary layer thickness. Substituting the expressions of δ and $A = r$ into the expression of the effective density, one obtains

$$\tilde{\rho}_e = \rho_0\tilde{\alpha} = \alpha_\infty\rho_0 \left(1 + \frac{2}{\rho_0\omega r} R_s \right) - j\alpha_\infty\rho_0 \frac{2}{\rho_0\omega r} R_s, \quad (5)$$

where $R_s = \frac{1}{2}\sqrt{2\eta\omega\rho_0}$ denotes the surface resistance.

The acoustic impedance at A' reads

$$Z_{A'} = \alpha_\infty \frac{2d}{r} R_s + j\rho_0\omega\alpha_\infty d + j\alpha_\infty \frac{2d}{r} R_s + \phi Z_B. \quad (6)$$

It is clearly seen that by using the following correction for the tortuosity:

$$\alpha_\infty = 1 + \frac{2\varepsilon_e}{d}, \quad (7)$$

the following impedance model is retrieved for the normal surface impedance in front of the panel $Z_A = Z_{A'}/\phi$:

$$Z_A = \left(\frac{2d}{r} + 4 \frac{\varepsilon_e}{r} \right) \frac{R_s}{\phi} + \frac{j\rho_0\omega}{\phi} (2\varepsilon_e + d) + j \left(\frac{2d}{r} + 4 \frac{\varepsilon_e}{r} \right) \frac{R_s}{\phi} + Z_B. \quad (8)$$

In the above equation, ε_e represents a correction length, which is a function of the perforation rate (or porosity) together with the perforation radius [5]. By making appropriate assumptions, both Allard Ingard and Beranek Ingard models [2] can then be reobtained from Eq. (8).

Allard Ingard model reads [5]

$$Z_A = \left(\frac{2d}{r} + 4 \right) \frac{R_s}{\phi} + \frac{j\rho_0\omega}{\phi} (2\varepsilon_e + d) + Z_B \quad (9)$$

with $\varepsilon_e = 0.48\sqrt{\pi r^2(1 - 1.14\sqrt{\phi})}$ and $\sqrt{\phi} < 0.4$.

Taking ε_e equal to r in the first term appearing in the resistance Eq. (8) and to $\varepsilon_e = 0.48\sqrt{\pi r^2(1 - 1.14\sqrt{\phi})}$ in the term $j\rho_0\omega/\phi(2\varepsilon_e + d)$, neglecting the term $j((2d/r) + 4(\varepsilon_e/r))R_s/\phi$ in the reactance, Eq. (9) is then reobtained.

Beranek Ingard’s model reads [2]

$$Z_A = \left(\frac{2d}{r} + 4\right) \frac{R_s}{\phi} + j \frac{\omega \rho_0}{\phi} (2\varepsilon_e + d) + j \left(\frac{2d}{r} + 4\right) \frac{R_s}{\phi} + Z_B \quad (10)$$

with $\varepsilon_e = 0.48\sqrt{\pi r^2}(1 - 1.47\sqrt{\phi} + 0.47\sqrt{\phi^3})$.

It is seen that Ingard in calculating the resistive part of the impedance in the perforation, assumed a different correction length than the one used for the inertial part. Basically, he assumed the distorted flow area to span half a sphere of radius r centered at the surface of the perforation.

If ε_e is taken equal to r in the first term appearing in the resistance Eq. (8) and in the term $j((2d/r) + 4(\varepsilon_e/r))R_s/\phi$ and if ε_e is taken equal to $0.48\sqrt{\pi r^2}(1 - 1.47\sqrt{\phi} + 0.47\sqrt{\phi^3})$ in the term $(j\rho_0\omega/\phi)(2\varepsilon_e + d)$ then Eq. (10) is reobtained.

Consider now the low-frequency limit of $\tilde{\rho}_e$ [5]

$$\tilde{\rho}_e = \rho_0 \tilde{\alpha} = \alpha_\infty \rho_0 \left(1 + \frac{2\alpha_\infty \eta}{\sigma A^2 \phi}\right) - j \frac{\sigma \phi}{\omega}. \quad (11)$$

The impedance in front of the perforated panel is given by, in terms of $A = r$ and the low-frequency (static) approximation of the flow resistivity, $\sigma = 8\eta/\phi r^2$

$$Z_A = \frac{1}{\phi} j \omega \tilde{\rho}_e d + Z_B = j \frac{\omega \rho_0}{\phi} d \alpha_\infty \left(1 + \frac{\alpha_\infty}{4}\right) + \sigma d + Z_B. \quad (12)$$

Usually the reactance term is negligible and $Z_A = \sigma d + Z_B$, which is the classical expression for resistive screens.

The previous expressions indicate that a rigid frame model can be used to model a perforated panel placed into two semi-infinite media as long as its geometric tortuosity is corrected to account for the effective length of the system. The proposed correction consists in adding the correction lengths to the panel tortuosity, which is equal to 1 for cylindrical perforations. The next section investigates the case where the perforated panel is backed by different acoustic systems and when it behaves as a resistive screen.

2.2. Case of perforated panels backed by a cavity: the Helmholtz resonator

Consider now a perforated plate backed by a cavity. The air layer between the plate and the rigid wall has a depth L . Under normal incidence, it is legitimate to assume that the air backing is partitioned. The system is known as a distributed Helmholtz resonator. Each cell represents a Helmholtz resonator with cavity volume V_{cav} , neck length d and neck aperture area A_{perf} . The volume is linked to the backing cavity depth L by $V_{\text{cav}} = A_{\text{perf}}L/\phi$. For sound at normal incidence, and for wavelengths larger than the lateral cavity dimensions, the normal surface impedance of the air layer is $Z_B = -j\rho_0 c_0 \cot(k_0 L)$, where ρ_0 is air density, c_0 is speed of sound and $k_0 = \omega/c_0$ is the wavenumber. The total input impedance of the perforated-air layer combination is

$$Z_A = \left(\frac{2d}{r} + 4\frac{\varepsilon_e}{r}\right) \frac{R_s}{\phi} + \frac{1}{\phi} (2\varepsilon_e + d) j \omega \rho_0 - j \rho_0 c_0 \cot(k_0 L). \quad (13)$$

The absorption coefficient is maximum at resonances occurring at zeros of the reactance term: $k_0 t g(k_0 L) = \phi/(2\varepsilon_e + d)$. At low frequencies, the wavelength is larger than the depth of the cavity and the first mode (resonance) is given by

$$\omega = \sqrt{\frac{c_0^2 \phi}{(2\varepsilon_e + d)L}} = \sqrt{\frac{c_0^2 A_{\text{perf}}}{(2\varepsilon_e + d)V_{\text{cav}}}}, \quad (14)$$

where $\phi/L = A_{\text{perf}}/V_{\text{cavity}}$ represents the ratio of the perforation area to the corresponding volume of the backing cavity, S is the cross-section of the cavity $\varepsilon_e = \varepsilon_0(1 - 1.14\sqrt{\phi})$ and $\varepsilon_0 = 8/3\pi\sqrt{A_{\text{perf}}/\pi} = 8r/3\pi = 0.48\sqrt{A_{\text{perf}}} = 0.85r$ is the radiation reactance of a circular, plane piston baffled in an infinite wall. The correction term $\varepsilon_e/\varepsilon_0$ accounts for interaction between the perforations.

This development shows that the resonance of the corresponding Helmholtz resonator [9] is retrieved from the equivalent fluid model, Eq. (8) for the perforations and backing cavity. Note that Panton and Miller [11] showed that for $L < \pi\lambda/16$, the resonance expression should be corrected to account for other terms in the low-frequency expansion of $\cot(k_0L)$. Using the first two terms, they gave the following expression:

$$\omega = \sqrt{\frac{c_0^2 A_{\text{perf}}}{(2\varepsilon_e + d)V_{\text{cav}} + (L^2 A_{\text{perf}}/3)}}. \quad (15)$$

Note that in the approach using an equivalent fluid model, Eq. (13), accounts exactly for the $\cot(k_0L)$ term.

Next section explains how the case of a perforated panel backed by an absorbing layer is treated with the proposed model.

2.3. Perforated plates in contact with a rigid frame porous layer

Since a rigid frame model is proposed to model the backing layer, the configuration represents the case where the perforated screen is not attached to the porous layer and free to move. Allard [5] gives a detailed analysis in Chapter 10 of his book. Here, one assumes that the main influence of the perforated screen is the distortion of the flow in the porous material, which creates an inertial effect, but also a resistive effect. As in the case of air, this distortion will be accounted for by a correction length resulting in an added reactance term, which depends on the porous layer tortuosity. Two correction terms to the surface impedance at the contact between the perforated screen and the backing porous material have been considered in this work. The first one writes $j\omega \text{Re}(\tilde{\rho}_p)\varepsilon_e$ with $\tilde{\rho}_p = \rho_0 \tilde{\alpha}_p$ the porous material's effective density; it depends on the real part of the dynamic tortuosity $\text{Re}(\tilde{\alpha}_p)$ of the porous layer together with ε_e the added length associated to the radiation in free air. The real part of the tortuosity, which is to be related to the path length, should be used rather than the complex valued tortuosity otherwise additional resistance effects are included. Using the complex-valued tortuosity would result in an overestimation of the absorption coefficient. The second correction terms writes $j\omega\rho_0\alpha_{\infty,p}\varepsilon_e$ and depends on the geometrical tortuosity of the porous layer $\alpha_{\infty,p}$ and ε_e has the same meaning as before.

If the first model is used, the resulting impedance at point B in front of the porous material, just at the rear of the perforated screen, is given by

$$Z_B = \frac{Z_{0,0}(B)}{\phi_p} + \frac{1}{\phi} j\omega \text{Re}(\tilde{\rho}_p)\varepsilon_e. \quad (16)$$

If the second model is applied, $\rho_0\alpha_{\infty,p}$ is substituted in Eq. (16) in place of $\tilde{\rho}_p$. In this equation $Z_{0,0}(B)$ is the normal surface impedance at point B in the absence of the perforated screen (the indices emphasizes the fact that only the normal mode is propagating), ϕ_p is the porosity of the porous layer in contact with the screen and $\tilde{\rho}_p$ its effective density. For example, if the porous layer has depth L and is backed by a rigid wall, $Z_{0,0}(B)$ is equal to $-jZ_c \cot(\tilde{k}_p L)$, where Z_c is the characteristic impedance and \tilde{k}_p is the wavenumber in the porous material. At point A in front of the screen outside the perforation, the surface impedance is given by

$$Z_A = \left(\frac{2d}{r} + 4\right) \frac{R_s}{\phi} + \frac{1}{\phi} (\varepsilon_e + d) j\omega\rho_0 + \frac{1}{\phi} j\omega \text{Re}(\tilde{\rho}_p)\varepsilon_e + \frac{Z_{0,0}(B)}{\phi_p}. \quad (17)$$

Expressing $\tilde{\rho}_p$ in terms of the dynamic tortuosity of the material: $\tilde{\rho}_p = \rho_0 \tilde{\alpha}_p$, the above expressions reads

$$Z_A = \left(\frac{2d}{r} + 4\right) \frac{R_s}{\phi} + \frac{1}{\phi} (\varepsilon_e(1 + \text{Re}(\tilde{\alpha}_p)) + d) j\omega\rho_0 + \frac{Z_{0,0}(B)}{\phi_p}. \quad (18)$$

In general, the viscous term is much smaller than the real part of the impedance of the porous material ($Z_{0,0}(B)$) and the impedance reduces to

$$Z_A = \frac{1}{\phi} (\varepsilon_e(1 + \text{Re}(\tilde{\alpha}_p)) + d) j\omega\rho_0 + \frac{Z_{0,0}(B)}{\phi_p}. \quad (19)$$

However, for the proposed model to handle the case where the perforated plate is in contact with an air layer, the viscous term should be kept. In conclusion, using an equivalent fluid model, the equivalent tortuosity should be taken equal to

$$\alpha_\infty(\omega) = 1 + \frac{\varepsilon_e}{d}(1 + \text{Re}(\tilde{\alpha}_p)), \tag{20}$$

when the first correction term is retained. If the static tortuosity correction term is adopted, then $\alpha_{\infty,p}$ should be substituted for $\text{Re}(\tilde{\alpha}_p)$ in Eq. (18)–(20). The relevance of the correction term is investigated in Section 3. It will be demonstrated that the dynamic correction term provides better results.

Note that Eq. (20) degenerates to Eq. (7) if the porous layer is replaced by an air gap (tortuosity $\tilde{\alpha}_p = 1$). Next section discusses how the proposed model deals with the case where the perforated panel is replaced by a resistive screen.

2.4. Case of a resistive screen

Resistive screen are acoustically characterized by their flow resistance R_s and their mass per unit area ρ_s . The impedance of the screen is given by: $Z_s = j\omega\rho_s R_s / (j\omega\rho_s + R_s)$. The above formula is only applicable when the screen is free to move due to pressure differential through it. When it is rigidly bonded onto a porous material, the inertial term is negligible and the impedance is simply given by $Z_s = R_s$. As seen in the section on perforated plates, the interaction impedance has also a reactance part accounting for the constriction of the oscillatory flow through the material. When backed by an absorber or a cavity, the surface impedance is the sum of the screen impedance and the absorber/cavity impedance: $Z_A = Z_s + Z_B$, where $Z_B = Z_{0,0}(B) / \phi_p$ for an absorbing material and $Z_B = -j\rho_0 c_0 \cot(k_0 L)$ for an air gap terminated by a rigid wall. In consequence, the modeling of perforated plates presented in the previous sections is applicable to resistive screens as long as the screen is free to move. However, since the resistive part of the resistance is mainly dominated by the flow resistivity of the screen, the impedance is given by

$$Z_A = \sigma d + \frac{1}{\phi}(\varepsilon_e(1 + \text{Re}(\tilde{\alpha}_p)) + d)j\omega\rho_0 + \frac{Z_{0,0}(B)}{\phi_p}. \tag{21}$$

For high flow resistivity thin screens, the reactance part is negligible and the classical flow resistive model is reobtained since $\sigma = R_s/d$.

2.5. Summary

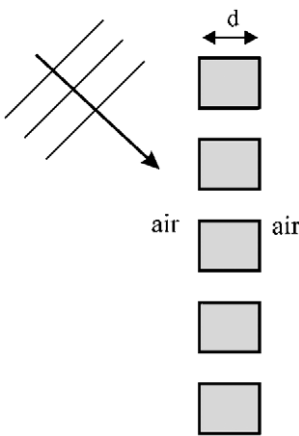
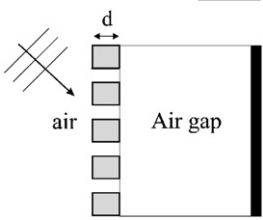
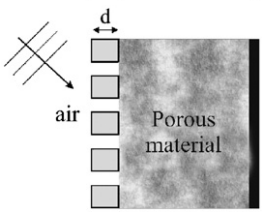
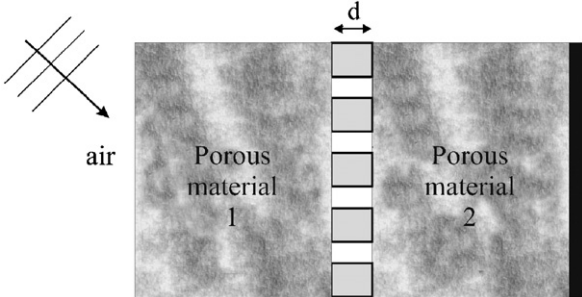
The previous sections have shown that perforated panels can be modeled using Johnson–Allard model for rigid porous media. The porosity ϕ , the flow resistivity σ and the characteristic lengths A , A' are calculated from the perforation rate and the size of the perforations. For circular cylindrical perforations of radius r , ϕ is simply the perforation rate, $\sigma = 8\eta/\phi r^2$, where η is the dynamic viscosity of air and $A = A' = r$. For resistive screens, the model is applicable as long as both the flow resistance and the porosity are measured. It will be shown in the example section that the classical model for resistive screens (i.e. simple addition of the resistance of the screen) is not sufficient.

In order to account for the distortion of the flow induced by the perforations, the tortuosity of the perforated panel must be corrected according to the media in which the perforated system radiates. The correction term is a function of the correction length associated to the radiation of a circular piston in free air noted ε_e together with the tortuosity of the medium in which the perforated panel radiated. In theory, it is only valid for normal incidence plane wave excitation. However, Allard [5] showed that the same correction lengths could also be used confidently at oblique incidence so that the proposed correction terms are suggested to be also used for this type of excitation. Table 1 summarizes the effective tortuosity to be used depending on the system attached to the perforated panel. In this table, for the case where the perforated screen is adjacent to a porous material, only the dynamic tortuosity correction term is shown since it is proved in Section 3 that it provides more reliable results than the static tortuosity correction term.

3. Validation and applications

This section presents validation results. The proposed approach is first compared with classical models of Beranek-Ingard, Maa and Allard (modal approach) [2,3,5], for normal incidence sound absorption performance. Then, normal incidence sound absorption experimental results carried out on multilayered systems of increasing complexity and comprising perforated panels are confronted to the results obtained from the present model. In the following, the properties of the different layers are displayed in Table 2.

Table 1
Summary of equivalent tortuosity expressions used in the proposed model

Configuration	Equivalent tortuosity
	$\alpha_{\infty}(\omega) = 1 + \frac{2\varepsilon_c}{d}$
	$\alpha_{\infty}(\omega) = 1 + \frac{2\varepsilon_c}{d}$
	$\alpha_{\infty}(\omega) = 1 + \frac{\varepsilon_c}{d} (1 + \text{Re}(\tilde{\alpha}_p)) \text{ (dynamic correction)}$
	$\alpha_{\infty}(\omega) = 1 + \frac{\varepsilon_c}{d} (\text{Re}(\tilde{\alpha}_{p,1}) + \text{Re}(\tilde{\alpha}_{p,2}))$

$\varepsilon_c = 0.48\sqrt{\pi r^2}(1 - 1.14\sqrt{\phi})$, where r is the perforation radius and ϕ the perforation rate.
 $\text{Re}(\tilde{\alpha}_{p,i})$: real part of the dynamic tortuosity of porous medium i .

3.1. Comparisons with existing models

Fig. 3 shows the normal incidence sound absorption coefficient of a 1 mm thick perforated panel referred to as panel 1 in Table 2 and backed by a 60 mm thick air gap. It compares (i) the present approach involving the tortuosity correction shown in Table 1, (ii) the rigid frame model for the perforated panel without tortuosity correction, (iii) Beranek Ingard’s and (iv) Maa’s models. Fig. 3 shows that the proposed tortuosity correction needs to be accounted for to predict correctly the position and the amplitude of the resonance peaks (compared with the rigid model in which the tortuosity is assumed equal to 1). Note that for air, the dynamic and static tortuosities are equal. Good agreement is found with classical models but the proposed correction underestimates the viscous dissipation on the first peak. However, its predictions are closer to the modal approach. The modal approach model considers the perforated panel as an assembly of elementary square cells of length D and infinite thickness to calculate the correction length in free air associated to the radiation of the aperture. The pressure field inside the cell is assumed to be stationary in the plane of the cell (expansion in terms of normal modes) and propagative along the thickness. At the aperture, the acoustic normal velocity is supposed to be of uniform amplitude. Applying boundary conditions, solving for the modal participation factors and introducing viscous dissipation inside the aperture and at the panel surface gives the normal

Table 2
Summary of the averaged measured properties of the materials used in the validations

	Porosity	Flow resistivity ($N s m^{-4}$)	Tortuosity	Viscous length (mm)	Thermal length (mm)	Bulk density ($kg m^{-3}$)
Panel 1 ($d = 1\text{ mm}$, $r = 0.5\text{ mm}$)	0.025	23440	NA	NA	NA	NA
Foam 1	0.99	10900	1.02	0.1	0.13	8.8
Foam 2	0.98	50000	1.5	0.034	0.13	20
Felt	0.94	23260	1.4	0.064	0.131	66
Panel 2 ($d = 20\text{ mm}$, $r = 1\text{ mm}$)	0.02	7325	NA	NA	NA	NA
Panel 3 ($d = 20\text{ mm}$, $r = 1\text{ mm}$)	0.01	14650	NA	NA	NA	NA
Leather screen ($d = 0.8\text{ mm}$)	0.06	17000	NA	NA	NA	NA
Black screen ($d = 0.47\text{ mm}$)	0.08	137000	NA	NA	NA	NA
White screen ($d = 0.4\text{ mm}$)	0.03	350000	NA	NA	NA	NA

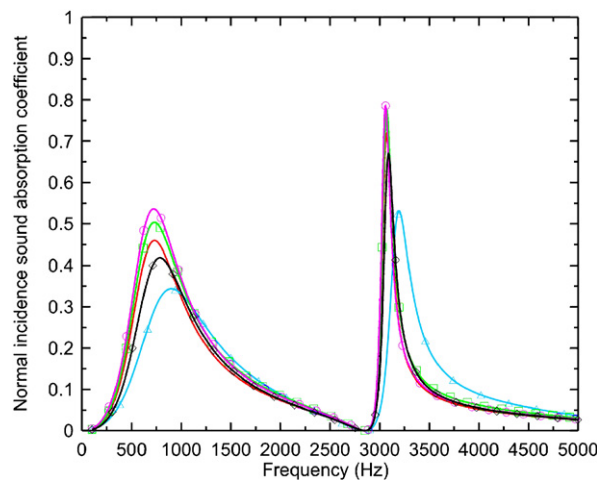


Fig. 3. Normal incidence sound absorption coefficient of a 1 mm thick perforated panel (panel 1) backed by a 60 mm thick air gap—comparisons between the present approach involving the tortuosity correction, rigid frame approach without tortuosity correction, Beranek Ingard’s and Maa’s models. —●—: Current approach—dynamic tortuosity correction, —▲—: rigid frame approach without tortuosity correction, —□—: Beranek Ingard, —○—: Maa, —○—: modal approach.

surface impedance at point *A* of the finite thickness panel [5]

$$Z_A = j \frac{\omega \rho_0}{\phi} (\varepsilon_e^1 + \varepsilon_e^2) + \left(\frac{2d}{r} + 4 \right) \frac{R_s}{\phi} + \frac{Z_{0,0}}{\phi_p}(B), \tag{22}$$

where ε_e^1 and ε_e^2 are the correction lengths in the air and in the porous medium, respectively

$$\varepsilon_e^1 = \sum_{(m,n) \neq (0,0)} v_{mn} \frac{2DJ_1^2(2\pi(r/D)(m^2 + n^2)^{1/2})}{\pi(m^2 + n^2)^{3/2}}, \tag{23}$$

$$\varepsilon_e^2 = 4 \sum_{m,n} v_{mn} \frac{J_1^2(2\pi(r/D)(m^2 + n^2)^{1/2})}{\pi(m^2 + n^2)} \frac{Z_{m,n}(B)}{\phi_p} \tag{24}$$

with $Z_{m,n}(B) = -jZ_c(k/k_{mn}) \cot(k_{mn}L)$ and $v_{m,n} = 1$ if $(m, n) \neq (0, 0)$; $v_{m,n} = 1/2$ if m or $n = 0$ and $v_{0,0} = 1/4$.

Fig. 4 depicts the normal incidence sound absorption coefficient of a 1 mm thick perforated panel referred to as panel 1 in Table 2 backed by a 20 mm thick low-flow resistivity foam (foam 1 in Table 2). It compares (i) the present approach involving the two tortuosity correction terms (dynamic and static) discussed in Section 2.3, (ii) the rigid frame model for the perforated panel without tortuosity correction, (iii) Beranek Ingard’s, (iv) Maa’s models and (v) modal approach model. Fig. 4 indicates that a good agreement is found between the proposed approach and classical models whether the dynamic or static tortuosity correction term is used. The static correction provides a better match with the classical models whereas the dynamic correction is in better agreement with the modal approach. Note that in the classical models, the correction length is the same whether the perforated panel radiates in air or in the porous material. The modification of the flow distortion induced by the presence of the material is therefore not accounted for. This explains the slight discrepancies between the current approach and the classical ones. Again, it is noticed that the tortuosity correction needs to be accounted for to predict correctly the position and the amplitude of the resonance peaks (see the rigid porous model in Fig. 4 which does not use the tortuosity correction).

Fig. 5 shows the normal incidence sound absorption coefficient of a 1 mm thick perforated panel (panel 1 in Table 2) backed by a 20 mm thick mid-flow resistivity foam (foam 2 in Table 2). On the one hand, there is a very good agreement between the modal approach (which accounts for the radiation of the perforated panel inside the porous material) and the present model when the dynamic tortuosity correction is used. On the

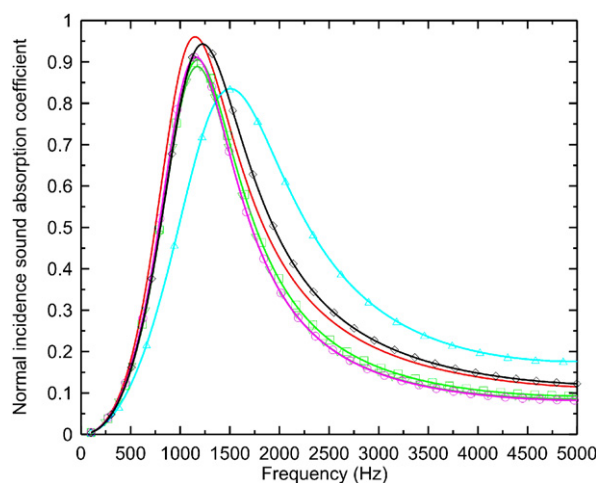


Fig. 4. Normal incidence sound absorption coefficient of a 1 mm thick perforated panel (panel 1) backed by a 20 mm thick low-flow resistivity foam (foam 1)—comparisons between the present approach (including dynamic and static corrections), rigid frame approach without tortuosity correction, Beranek Ingard’s, Maa’s and modal approach’s models. —●—: Current approach—dynamic tortuosity correction, —▲—: Rigid frame approach without tortuosity correction, —□—: Beranek Ingard, —○—: Maa, —●—: Modal approach, —▽—: Current approach—static tortuosity correction.

other hand, the static tortuosity correction gives the same trends as the classical models. These observations were also made in the previous case. Compared to low flow resistivity foam, increased differences are noticed between classical models and the proposed one. Since the foam has a higher flow resistivity than that used in Fig. 4, the distortion of the flow is more important and induces a larger difference between the classical correction length in free air and the one which accounts for the radiation in the backing porous layer. This is even more important for highly resistive backing materials, In consequence, the classical models are not accurate for such configurations. Recourse to a modal approach or the proposed modeling approach is suggested.

The proposed model has been tested in various other configurations. For example, it has also been found to predict extremely well sound absorption performance of $\frac{1}{4}$ wavelength resonators and Helmholtz resonators.

3.2. Comparisons with experimental results

In this section, the results obtained with the proposed model are confronted to normal incidence sound absorption coefficient measurement results.

Firstly, consider the case of a multilayered system made up of perforated panels and air cavities. The configuration of interest described in Ref. [8] consisting of a system made up of a 20 mm thick perforated panel referred to as panel 2 in Table 2, a 30 cm thick air gap, a 20 mm thick perforated panel referred to as panel 3 in Table 2 terminated by a 60 cm thick air gap. The experimental data have been obtained by the authors of paper [8]. Fig. 6 compares the sound absorption coefficient measured in a 2 m wide square rectangular reinforced concrete chamber operating as an acoustic waveguide below 80 Hz (see Fig. 11 in [8]), the results based on Maa’s approach (see Fig. 11 in [8]) together with the present model. It is seen that the proposed approach is in very good agreement with the measurements. In addition, it captures the physics better than Maa’s model.

In what follows, the tests have been carried out in a classical standing wave tube following ASTM E 1050-90.

Consider now three different resistive perforated screens attached to foam 1 (melamine). The screens have been chosen with increasing resistance. The first screen is a 0.8 mm thick leather perforated screen used in the automotive industry. The perforation radii are large (0.75 mm) and easily measurable. The other two screens are perforated scrims and their perforation rates have been estimated from an inverse characterization method involving the normal incidence absorption of the screen with a backing cavity. Figs. 7–9 show the measured

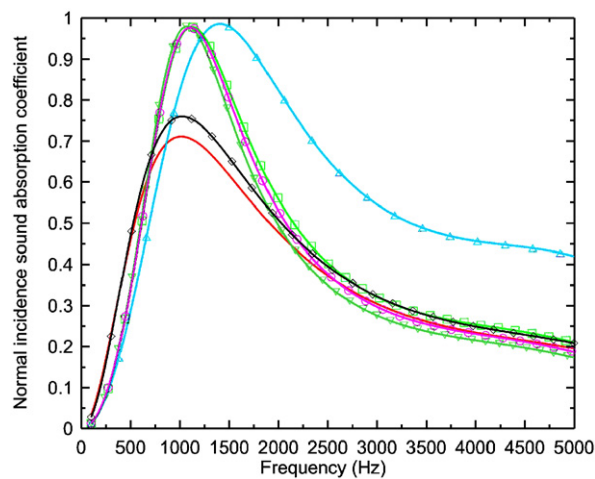


Fig. 5. Normal incidence sound absorption coefficient of a 1 mm thick perforated panel (panel 1) backed by a 20 mm thick mid-flow resistivity foam (foam 2)—comparisons between the present approach (including dynamic and static corrections), rigid frame approach without tortuosity correction, Beranek Ingard’s, Maa’s and modal approach’s models. —: Current approach—dynamic tortuosity correction, —△—: rigid frame approach without tortuosity correction, —□—: Beranek Ingard, —○—: Maa, —◇—: modal approach, —▽—: current approach—static tortuosity correction.

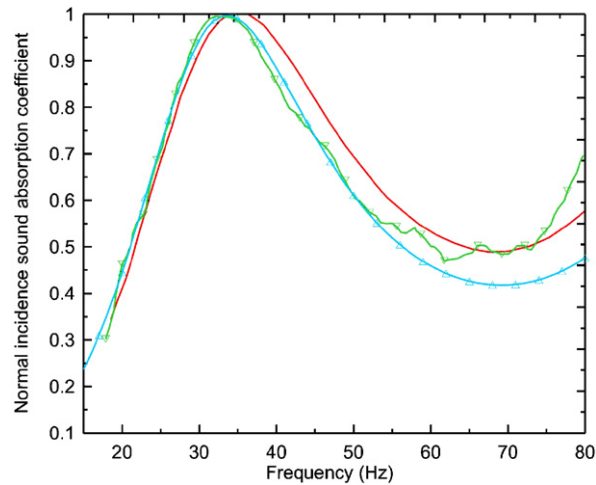


Fig. 6. Normal incidence sound absorption coefficient of a system made up of a 20 mm thick perforated panel (panel 2), a 30 cm thick air gap, a 20 mm thick perforated panel (panel 3) terminated by a 60 cm thick air gap [8]: comparisons between experimental results and models. —: Theoretical model Fig. 11 [11], — ∇ —: measurements Fig. 11 [11], — \triangle —: present approach.

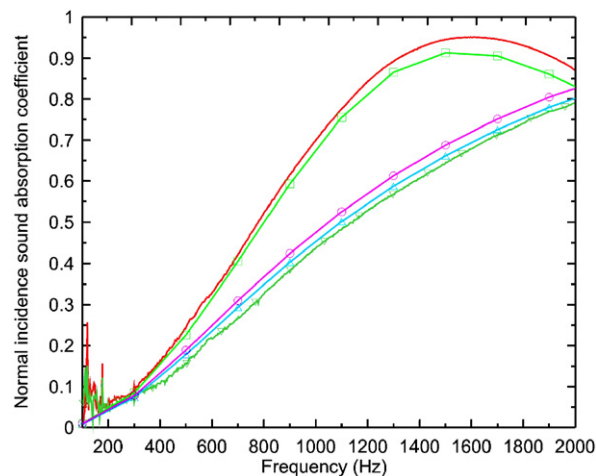


Fig. 7. Normal incidence sound absorption coefficient of a perforated screen (leather screen, $\sigma = 17\,000\text{ N s m}^{-4}$) backed by a 27 mm foam (foam 1): comparisons between experimental results and models. —: Test—foam + leather screen, — ∇ —: test—foam, — \triangle —: prediction—foam, — \square —: prediction—perforated screen model, — \circ —: prediction—resistive screen model.

normal incidence sound absorption coefficients of the foam and the foam with the attached screens. Also, in each case, a purely resistive model for the screen is shown and compared to the proposed model. The effects of the screens on this low-resistivity foam are clearly seen especially, at low frequencies. Moreover, it is shown that a purely resistive model is not sufficient when the flow resistance of the screen is low. The reactance and resistance resulting from the restrictions of flow through the screens perforations must be accounted for. However, as the screen flow resistance increases the simple resistance model becomes acceptable.

The normal incidence sound absorption coefficient of a perforated screen inserted between two materials is now investigated. A black screen is inserted between a 27 mm foam (foam 1 in Table 2) and a 19 mm felt material. The results are presented in Fig. 10. This figure indicates that the effect of the screen on the felt and foam alone is well predicted. When the perforated screen is inserted between the two porous layers, the proposed model proves also to accurately predict the acoustic performance of the assembly. Again, the simple resistive model fails to correctly capture the screen effect.

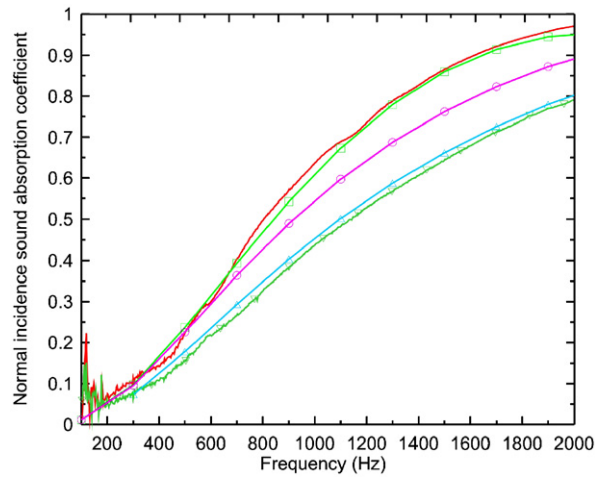


Fig. 8. Normal incidence sound absorption coefficient of a perforated screen (black screen, $\sigma = 137\,000\text{ N s m}^{-4}$) backed by a 27 mm foam (foam 1): comparisons between experimental results and models. —: Test—foam + black screen, —▽: test—foam, —△: prediction—foam, —□: prediction—perforated screen model, —○: prediction—resistive screen model.

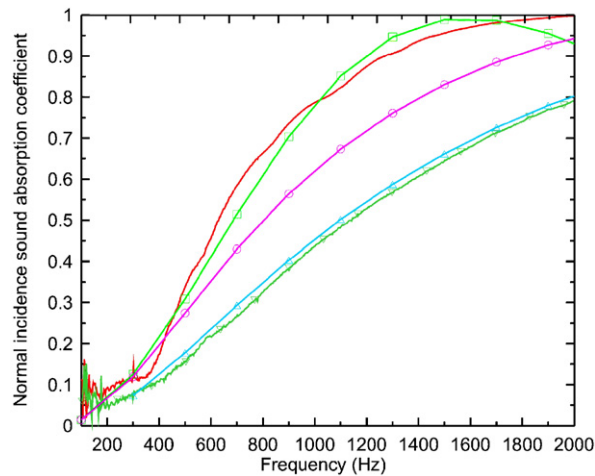


Fig. 9. Normal incidence sound absorption coefficient of a perforated screen (white screen, $\sigma = 350\,000\text{ N s m}^{-4}$) backed by a 27 mm foam (foam 1): comparisons between experimental results and models. —: Test—foam + white screen, —▽: test—foam, —△: prediction—foam, —□: prediction—perforated screen model, —○: prediction—resistive screen model.

4. Conclusion

This paper presented a simple and general model that can handle easily and automatically miscellaneous configurations involving perforated plates and screens. The perforated panel model is based on the use of the Johnson–Allard model for rigid porous media with an effective tortuosity. This effective tortuosity is shown to depend on a correction length, which is a function of the correction length induced by the radiation of the perforated screen in free air and of the dynamic tortuosity of the media interfacing with the perforated system. This dynamic tortuosity is obtained from the real part of Johnson’s complex dynamic tortuosity.

Comparisons with existing models and experimental results for various configurations involving perforated screens added to air gap, to porous layer or inserted between two porous layers have been shown to corroborate the validity of the proposed model. The presented results show that this model is capable of handling perforated plates or screens backed by cavities filled with acoustic materials. Classical models for

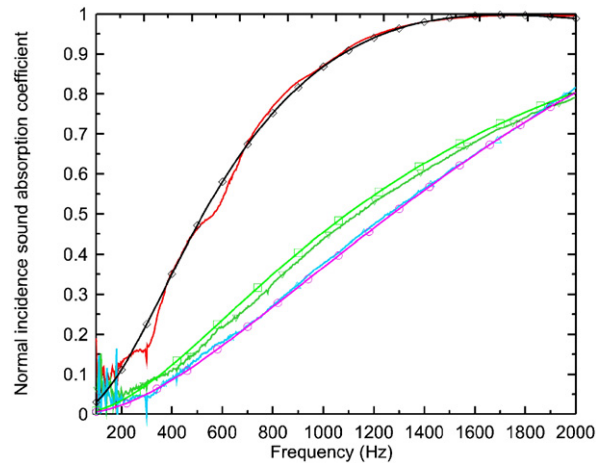


Fig. 10. Normal incidence sound absorption coefficient of a perforated screen (black screen, $\sigma = 137\,000\text{ N s m}^{-4}$) backed by a 27 mm foam (foam 1), a 19 mm felt or inserted between the two: comparisons between experimental results and models. —: Test—felt + black screen + foam, — ∇ —: test—foam, — \triangle —: Test—felt, — \square —: prediction—foam, — \circ —: prediction—Felt, — \circ —: prediction—perforated screen model.

both perforated plates and screens including sub-millimeter perforations configurations can be retrieved using this simple approach. In addition, the mass of the perforated screen or perforated plate can also be accounted for by extending the model to include the inertia of the solid phase (limp version of the equivalent fluid model). The other advantage of the method is that it is general. In particular, it is not necessary to develop a specific model for a perforated system. All the existing models (macro- and microperforated) can be obtained from an equivalent fluid model by selecting appropriate parameters. Most transfer matrix softwares already include porous materials models but perforated systems require specific formulations. The implementation of this approach is therefore straightforward.

References

- [1] K.U. Ingard, *Notes on Sound Absorption Technology*, Noise Control Foundation, New York, 1994.
- [2] L.L. Beranek, I.L. Ver, *Noise and Vibration Control Engineering*, Wiley, New York, 1992.
- [3] D.Y. Maa, Microperforated wideband absorbers, *Noise Control Engineering Journal* 29 (3) (1987) 77–84.
- [4] J. Kang, H.V. Fuchs, Predicting the absorption of open weave textiles and microperforated membranes backed by an airspace, *Journal of Sound and Vibration* 220 (5) (1999) 905–920.
- [5] J.F. Allard, *Propagation of Sound in Porous Media*, Elsevier, London, 1993.
- [6] F. Mechel, *Formulas of Acoustics*, Springer, Berlin, 2002 (p. 1175).
- [7] D. Takahashi, A new method for predicting the sound absorption of perforated absorber systems, *Applied Acoustics* 51 (1) (1997) 71–84.
- [8] J. Lee, G.W. Swenson, Compact sound absorbers for low frequencies, *Noise Control Engineering Journal* 38 (3) (1992) 109–117.
- [9] R.T. Randeberg, Perforated Panel Absorbers with Viscous Energy Dissipation Enhanced by Orifice Design, PhD Thesis, Trondheim, 2000.
- [10] N. Atalla, F. Sgard, Y. Atalla, On the modeling of perforated plates and screens, *12th ICSV*, Lisbon, July 2005.
- [11] R.L. Panton, J.M. Miller, Resonant frequencies of cylindrical resonator, *Journal of the Acoustical Society of America* 57 (6 II) (1975) 1533–1535.